


## Article

# Orientation Selection of Supported Au Nanoparticles on (111)- and (001)-Terminated SrTiO<sub>3</sub> Substrates

Wangwang Kuang<sup>1,2</sup> and Guozhen Zhu<sup>1,\*</sup> 

<sup>1</sup> Department of Mechanical Engineering and Manitoba Institute for Materials, University of Manitoba, Winnipeg, MB 147000, Canada

<sup>2</sup> State Key Laboratory of Metal Matrix Composites, School of Materials Science and Engineering, Shanghai Jiao Tong University, 800 Dongchuan Rd., Shanghai 200240, China

\* Correspondence: guozhen.zhu@umanitoba.ca

**Abstract:** Orientation-dependent performance has been demonstrated in different materials consisting of nanoparticles on substrates. The fabrication of desirably oriented nanoparticles requires knowledge of orientation selection rules. Based on the Wulff–Kaishe theory, our analysis shows that the energy-favorable orientation(s), is influenced by the surface energy of particles, in addition to the dominant factor, i.e., the energy difference between particle/substrate interfacial energy and surface energy of the substrate. To verify this, a model system of dewetted Au nanoparticles on SrTiO<sub>3</sub> is studied. The {111}-terminated SrTiO<sub>3</sub> supports only {111}-orientated Au particles, with the lowest interfacial energy. On the other hand, {100}-terminated SrTiO<sub>3</sub> supports multiple Au particles, with {111}-, {100}-, {110}- orientations, as a possible result of close surface energy contributions. The above orientations can be additionally manipulated by changing the heat treatment temperature. Our results provide fundamental insights into fabricating supported nanoparticles for practical applications.

**Keywords:** gold-oxide nanostructure; interfacial energy; orientation selection; catalytic; Wulff–Kaishe theory



**Citation:** Kuang, W.; Zhu, G.

Orientation Selection of Supported Au Nanoparticles on (111)- and (001)-Terminated SrTiO<sub>3</sub> Substrates. *Crystals* **2022**, *12*, 1414. <https://doi.org/10.3390/cryst12101414>

Academic Editor: Pavel Lukáč

Received: 17 August 2022

Accepted: 3 October 2022

Published: 6 October 2022

**Publisher's Note:** MDPI stays neutral with regard to jurisdictional claims in published maps and institutional affiliations.



**Copyright:** © 2022 by the authors. Licensee MDPI, Basel, Switzerland. This article is an open access article distributed under the terms and conditions of the Creative Commons Attribution (CC BY) license (<https://creativecommons.org/licenses/by/4.0/>).

## 1. Introduction

Supported nanoparticles, particularly on oxides, have attracted abundant attention for their enormous catalytic [1,2], electrical [3,4], and photovoltaic [5,6] applications. In addition to those well-studied factors, such as particle size and facets, how nanoparticles orient on the substrate, in terms of their crystallographic characteristics, largely determines the synergetic performance of nanoparticles and supports, and therefore, can further promote their applications. This is because the alignment between the metal and oxide lattices (i.e., their orientation relationships) governs the interface structure and charge transferred across the interface, given the structural origins for their unique physical and chemical properties. For example, orientation-dependent enhancement in catalytic performance is demonstrated in Pd/TiO<sub>2</sub> [7] and Pd/SrTiO<sub>3</sub> [8]. A tunable Schottky barrier is discovered in differently oriented Au nanoparticles on SrTiO<sub>3</sub> [4,9]. Enhanced photocatalytic performance has been reported with special crystallographic orientations in Au/SrTiO<sub>3</sub> [10]. Thus, it is technically important to understand how to tune the orientations of supported nanoparticles, to achieve controllable fabrication of supported nanoparticles.

Without the substrate, particles likely maintain equilibrium shapes with minimized energy, which can be well defined by the Wulff construction [11] and its atomistic modifications [12,13]. With a rigid flat substrate, supported particles, at a given orientation, have energy minimization with equilibrium shape (i.e., Wulff–Kaishe shape [14,15]), describing the substrate effect as interfacial energy contribution with/without stress effect [16]. Such substrate effect is strongly linked to the orientation and the associated interface structure between the nanoparticles and the substrate. On the other hand, preferential interfaces with low interfacial energy are experimentally discovered and theoretically predicted for target

nanoparticles on substrates, and are adopted to explain multiple observed orientations of supported particles [17–19]. Despite extensive investigations on supported nanoparticles and their orientations, few studies have addressed the orientation selection of supported nanoparticles, particularly when different interfaces have close interfacial energy.

With an isotropic substrate, supported nanoparticles have orientation-dependent nucleation barriers [20]. This theoretical prediction can be utilized to guide the synthesis of target-oriented nanoparticles by tuning the interfacial energy with additional chemical entities on the substrate surface. It should be noted that the orientation of supported nanoparticles can be modified at elevated temperatures during the calcination, which is likely involved after deposition or “bottom-up” methods of synthesizing supported nanoparticles. Moreover, the anisotropic nature of most oxide substrates has the possibility of tailoring the interfacial energy with different surface terminations [7–10] and surface reconstructions [21], and consequently, provides large room for tuning the orientation of nanoparticles using “clean” metal oxide systems.

Accordingly, a quantitative description of orientation selections for supported nanoparticles, as a result of energy minimization, can be a valuable guide for fabricating supported nanoparticles in a controllable fashion. Herein, we compare the energy of supported particles with different orientations, quantifying the contribution of the surface energy of particles, in addition to the key parameter involving interfacial energy, as concluded in the literature [14–16]. Furthermore, we experimentally verify our theoretical predictions, and additionally demonstrate the possibility of manipulating the orientation of supported nanoparticles on the substrate with different surface terminations. Our results provide insights into the design of supported nanoparticles.

## 2. Materials and Methods

To validate the theoretical prediction of orientation selection, Au nanoparticles supported on SrTiO<sub>3</sub> substrates were synthesized using the thermal dewetting method. In detail, gold films with a thickness of 5–10 nm, were sputtered on the (111)- and (100)-oriented SrTiO<sub>3</sub> single crystal substrates (purchased from MTI corporation, Richmond, CA, USA), respectively. Before the gold deposition process, substrates were thoroughly rinsed and carefully cleaned with organic solvents. Afterward, gold-deposited substrates were sealed in a quartz tube filled with an argon atmosphere in order to avoid any possible contamination during the subsequent annealing route. Samples were then heated to 800, 900, 1000, and 1100 °C for 1 h at a heating rate of 5 °C/min in a tube furnace filled with argon atmosphere until they cooled down to room temperature in the furnace.

The crystallography of dewetted gold nanoparticles was investigated by the X-ray diffraction technique using a Bruker discover X-ray powder diffractometer (XRD). With the advantage of two-dimensional detectors, {111}<sub>Au</sub> and {200}<sub>Au</sub> pole figures were produced from the same scanning sequence in order to facilitate the analysis of orientation. The interpretation of the pole figures was performed by comparing the experimental data with the simulated pole figures from Matlab codes (Matlab 2019a). (More experimental details in Supplementary Materials).

## 3. Results and Discussion

### 3.1. Criterion of Orientation Selection

The equilibrium morphology of a crystalline particle, supported on a substrate, can be conceptually described as the minimization of total energy, herein mainly referring to the surface and interfacial energy. According to the Winterbottom construction [15], the substrate effect on the equilibrium shape of a particle can be treated as an intersecting line of the Wulff plot of this particle. For example, a two-dimensional (2D) particle, with a cubic lattice, has a Wulff plot in the shape of a four-leaf clover (see the blue curve in Figure 1a) and its equilibrium shape as the inner convex hull (the black curve in Figure 1a). When a substrate, e.g., A, B, or Z, intersects with this cubic particle, its equilibrium shape becomes

a truncated square. The change in the total surface and interfacial energy of this particle, after introducing a given substrate, can be defined as:

$$\Delta E = \gamma_P \Delta S_P + (\gamma_I - \gamma_S) \Delta S_I \quad (1)$$

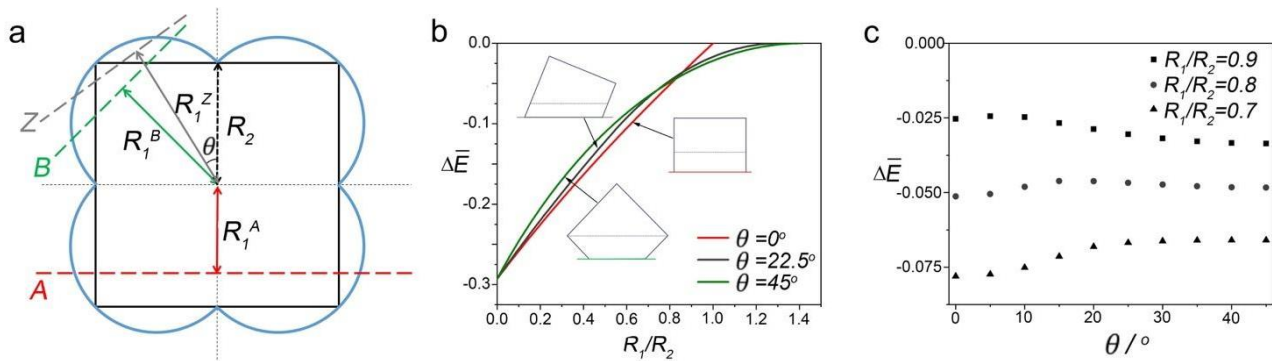


**Figure 1.** Equilibrium shape and the change in the total energy of a two-dimensional particle. (a) the schematic diagram of Wulff–Kaishew construction; (b) The evolution of the change in the normalized total energy  $\Delta \bar{E}$  with the  $R_1/R_2$  ratio for selected orientations; and (c) the evolution of  $\Delta \bar{E}$  with interface orientation for given  $R_1/R_2$  ratios.

Here  $\gamma_P$ ,  $\gamma_I$ ,  $\gamma_S$  represent the energy of the particle surfaces, interface, and substrate surface per unit area, respectively, and  $\Delta S_P$  and  $\Delta S_I$  are the changes in the total area of the particle surface and interface, because of the intersection of a given substrate, respectively. Accordingly, the Kaishew theorem describes the equilibrium shape of a supported particle as (Wulff–Kaishew shape [14,15])

$$\frac{R_1}{R_2} = \frac{\gamma_I - \gamma_S}{\gamma_P} \quad (2)$$

Herein,  $R_1$  and  $R_2$  are the distances from the Wulff center to the interface and to the particle facet, respectively. Since  $\gamma_P$  and  $\gamma_S$  are known parameters for a given material system, the interfacial energy  $\gamma_I$  can be directly obtained by measuring the shape of the particle. Under the assumption of a constant area of this 2D particle (i.e., constant volume in 3D), the change in the total energy  $\Delta E$  is a function of  $R_1/R_2$  ratio for any given orientation, as shown in Figure 1b. For simplicity,  $\Delta E$  is normalized to the total surface energy of the particle with its Wulff shape, defined as  $\Delta \bar{E}$  in the following discussion. The total energy is found to decrease continuously with gradual cutting into the particle (shown by decreasing  $R_1/R_2$ ). This suggests that interfacial energy  $\gamma_I$ , or to be precise, the energy difference  $\gamma_I - \gamma_S$ , plays a significant role in the modifying of equilibrium particle shape by the substrate, as concluded in the literature [15].

Targeting orientation-dependent performance, the more critical issue is how to control the orientation and subsequent shape of particles. This can be deemed as the changing tendency in the total energy of a supported particle when the intersected interface tilts at an arbitrary angle, which is defined as  $\theta$  in Figure 1a. The normalized change in the total energy  $\Delta \bar{E}$  is orientation-dependent, shown as different curves for selected orientations in Figure 1b. Within a wide range of  $0 \leq R_1/R_2 \leq \sim 0.8$ ,  $\theta = 0^\circ$  gives rise to the largest reduction in the total surface/interface energy. Physically, the case of  $\theta = 0^\circ$  implies the fact that the close-packed plane of “atoms” of the particle with a 2D cubic lattice (i.e., usually has a low surface energy and is the facet) parallels the substrate surface, probably leading to the interface with the lowest energy. In general, the case of  $\theta = 0^\circ$  likely maintains low interfacial energy, and at the same time, is the energetically favorable orientation for a wide range of  $R_1/R_2$  ratios. It should be noted that  $R_1$  can also be negative when the interfacial energy  $\gamma_I$  is smaller than the surface energy of substrate  $\gamma_P$  (see the Supplementary Materials).

Figure 1c presents the variation of  $\Delta\bar{E}$  for a given interfacial energy, which equals to a given  $R_1/R_2$  ratio since  $\gamma_S$  and  $\gamma_P$  are constant. To further quantify the orientation-dependent differences of  $\Delta\bar{E}$ , a few typical  $R_1/R_2$  ratios are selected according to the commonly reported experimental observations [18,22]. The case of  $\theta = 0^\circ$  has the lowest value of  $\Delta\bar{E}$  when  $R_1/R_2 = 0.7$  and  $0.8$ . When  $R_1/R_2 = 0.9$ , the case of  $\theta = 45^\circ$  maintains the lowest  $\Delta\bar{E}$ . This fact suggests that the surface energy contribution of a particle can change its orientation, particularly when this nanoparticle is loosely bonded to the substrate (i.e., a large  $\gamma_I$ ). By contrast to this 2D particle, 3D (three-dimensional) particles have complex shape and different sets of facets, and therefore, can have the possibility of co-existing orientations with very close interfacial energy.

The aforementioned concept is extended to 3D particles with a face-center cubic (FCC) lattice as for many catalytic particles (e.g., Au, Pt, Pd, Ag). An FCC particle generally has its Wulff construction as a truncated octahedron, consisting of edge-joined hexagonal ( $\{111\}$ ) and square ( $\{100\}$ ) facets [22,23]. The truncated octahedron changes its area ratio of hexagonal and square facets, depending on the surface energy ratio of  $\{111\}$  and  $\{100\}$  ( $\gamma_{\{111\}}/\gamma_{\{100\}}$ ). To access the influence of its shape, three precious metals, Au, Pd, and Ag, are chosen with a decreasing tendency of hexagonal facets (e.g., an increasing tendency of ( $\gamma_{\{111\}}/\gamma_{\{100\}}$ ) according to reported values [24] (i.e.,  $\gamma_{\{111\}}^{Au} = 1.283 \text{ J/m}^2$ ,  $\gamma_{\{100\}}^{Au} = 1.627 \text{ J/m}^2$ ,  $\gamma_{\{111\}}^{Pd} = 1.920 \text{ J/m}^2$ ,  $\gamma_{\{100\}}^{Pd} = 2.326 \text{ J/m}^2$ ,  $\gamma_{\{111\}}^{Ag} = 1.172 \text{ J/m}^2$ ,  $\gamma_{\{100\}}^{Ag} = 1.200 \text{ J/m}^2$ ). Using the total surface energy of particles with Wulff shape as the reference, the normalized change in the total energy  $\Delta\bar{E}$  with three typical orientations is applied to quantify the orientation differences. The three typical orientations are  $\{111\}$ -,  $\{100\}$ -, and  $\{110\}$ -oriented particles, that is, interfaces parallel to the  $\{111\}$ ,  $\{100\}$ , and  $\{110\}$  planes of FCC lattice (see different morphologies in Figure 2a). All symbols maintain the same definitions as the two-dimensional case, and  $R_1$  and  $R_2$  are the distances from the Wulff center to the interface and  $\{111\}$  facet (i.e., the close-packed plane of “atoms”), respectively. The particle volume is constant when the substrate is cutting into the particle.

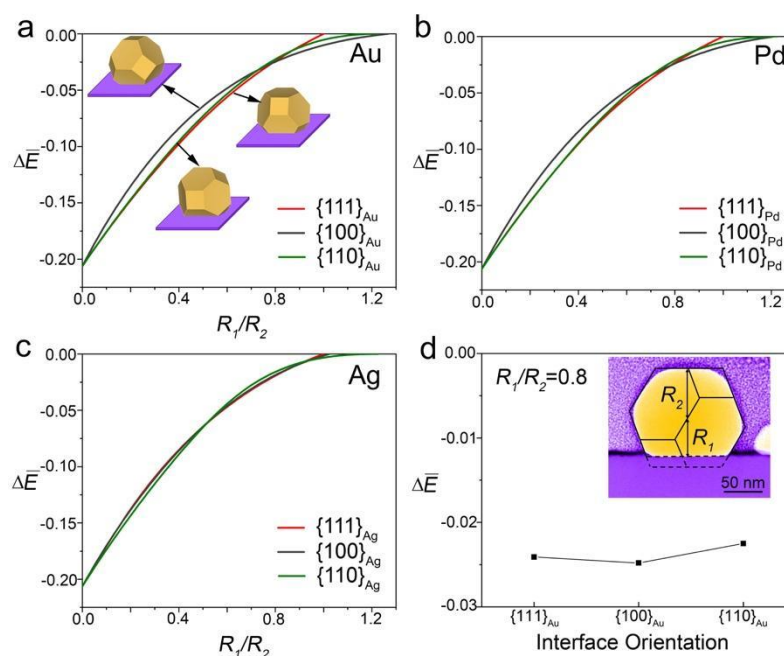


**Figure 2.** The change in the total energy of an FCC particle. (a–c) The evolution of normalized energy  $\Delta\bar{E}$  with  $R_1/R_2$  ratio for different interface orientations for Au, Pd, and Ag, respectively. In (a), the morphology of differently oriented Au particles is inserted to label the different curves. (d) the normalized energy  $\Delta\bar{E}$  for differently oriented Au particles for a fixed  $R_1/R_2$  ratio of 0.8.

The normalized changes in its total energy  $\Delta\bar{E}$  show similar characteristics to these of 2D particles: (1) for a given orientation, the energy reduction decreases as the substrate

cuts deeper into the particle; and (2) the decreasing tendency of  $\Delta\bar{E}$  varies with different orientations. In addition, the detailed shape of 3D particles affects the decreasing tendency of  $\Delta\bar{E}$ , demonstrated as the differences in Figure 2a-c. With a small  $\gamma_{\{111\}}/\gamma_{\{100\}}$  ratio (see Au and Pd in Figure 2a,b), particles with different orientations are favorable for different  $R_1/R_2$  ranges. The  $\{111\}$ - and  $\{100\}$ -oriented particles are preferred when  $R_1/R_2$  ratios are  $\sim 0.3$ – $0.8$  and  $> \sim 0.8$ , respectively. When  $R_1/R_2 < \sim 0.3$ , particles also prefer their interfaces parallel  $\{110\}$ , which has a higher surface energy compared to  $\{100\}$  and  $\{111\}$  and does not appear as a facet. On the other hand, with a large  $\gamma_{\{111\}}/\gamma_{\{100\}}$  ratio (see the Ag case in Figure 2c), particles with different orientations are very competitive. The  $\{111\}$ -oriented particles are slightly favorable over a  $R_1/R_2$  ratio of  $\sim 0.5$ – $0.9$ , and  $\{100\}$ -oriented particles are preferred over a  $R_1/R_2$  ratio of  $< 0.4$ . Again,  $R_1$  can be negative, and the details are in the Supplementary Materials.

For these three orientations, the total energy  $\Delta\bar{E}$  has very close values at a few interesting  $R_1/R_2$  ratios, for example,  $\sim 0.8$  for Au (see Figure 2d). This suggests the possibility of achieving energetically stable particles, with different orientations,  $\Delta\bar{E}$ , and such particles (for example,  $\{110\}$ -oriented particles) can have more edge atoms and more low-coordinated atoms at the perimeters, essential for their catalytic applications.

### 3.2. Experimental Validation Using Dewetted Au Nanoparticles on $\{111\}$ - and $\{001\}$ -Terminated $\text{SrTiO}_3$ Substrates

The special  $R_1/R_2$  ratio of approximately 0.8 has been reported in Au/ $\text{SrTiO}_3$  [10,22,25] and is additionally confirmed by our experimental measurement (as shown in the insert in Figure 2d). Accordingly, we selected this special system to further verify that i) particle orientation is primarily determined by its interfacial energy; and ii) multiple orientations can be favorable under certain conditions, such as similar contributions of interfacial energy (for example, an  $R_1/R_2$  ratio of 0.8) and similar contributions of the surface energy of a particle. The morphology of supported Au nanoparticles was investigated using scanning electron microscopy (see Figure S3 in the Supplementary Materials for more details). The size of these supported Au nanoparticles increases with increasing initial film thickness and heat treatment temperature, as reported in our previous work [22,23]. Although the observed facets and cross-sectional micrographs may also suggest the orientations of individual supported particles, XRD pole figures provide statistical representations of a huge number of Au particles and were applied here to access the orientations of supported Au particles.

With  $\{111\}$ -terminated substrates, Au particles maintain strong  $\{111\}$ -orientations when subjected to the heat treatment of  $800^\circ\text{C}$  to  $1100^\circ\text{C}$ , and have a random in-plane alignment (with a ring shape in Figure 3a), except at  $1100^\circ\text{C}$ , which has one main preferential orientation relationship (OR') of  $\{111\}_{\text{Au}} // \{111\}_{\text{SrTiO}_3} \& \langle 1\bar{1}0 \rangle_{\text{Au}} // \langle 1\bar{1}0 \rangle_{\text{SrTiO}_3}$  (shown as the six bright poles in experimental pole figure and the red stars in simulation in Figure 3a). The appearance of additional poles at  $1100^\circ\text{C}$  is from another preferential orientation relationship of  $\{115\}_{\text{Au}} // \{111\}_{\text{SrTiO}_3} \& \langle 1\bar{1}0 \rangle_{\text{Au}} // \langle 1\bar{1}0 \rangle_{\text{SrTiO}_3}$ , the twinned orientation of the main OR'. (Also see the black diamond in the simulation in Figure 3a.) Twins are frequently observed under such conditions [26,27], and the effect of twins is beyond the scope of the current discussion. Considering the lattice parameter for Au is  $4.078 \text{ \AA}$ , and for  $\text{SrTiO}_3$  it is  $3.905 \text{ \AA}$ ,  $\{111\}$ -oriented Au particles have the interface with better lattice matching compared to other orientations, implying a low interfacial energy. In addition, OR' matches between the close-packed directions and close-packed planes of two lattices, representing the interface with the lowest energy since no atomic reconstruction as a sign of strong bonding between Au and  $\text{SrTiO}_3$  is detected [22]. As demonstrated in atom-resolved STEM-HAADF (scanning transmission electron microscopy-high angle annular dark field) images in Figure 4, the Au/ $\text{SrTiO}_3$  OR' interface has no atomic reconstruction and is an atomically flat interface. Although the above epitaxy leads to a compressive strain of 4.4%, the coherent interface is expected to maintain low interface energy compared to other orientations with semi-coherent interfaces. At  $1100^\circ\text{C}$ , Au atoms have high mobility, leading

to the in-plane alignment of both lattices and the formation of OR'. In short, the matching of both lattices suggests the interface with the lowest energy, and ultimately determines the orientation of Au particles.

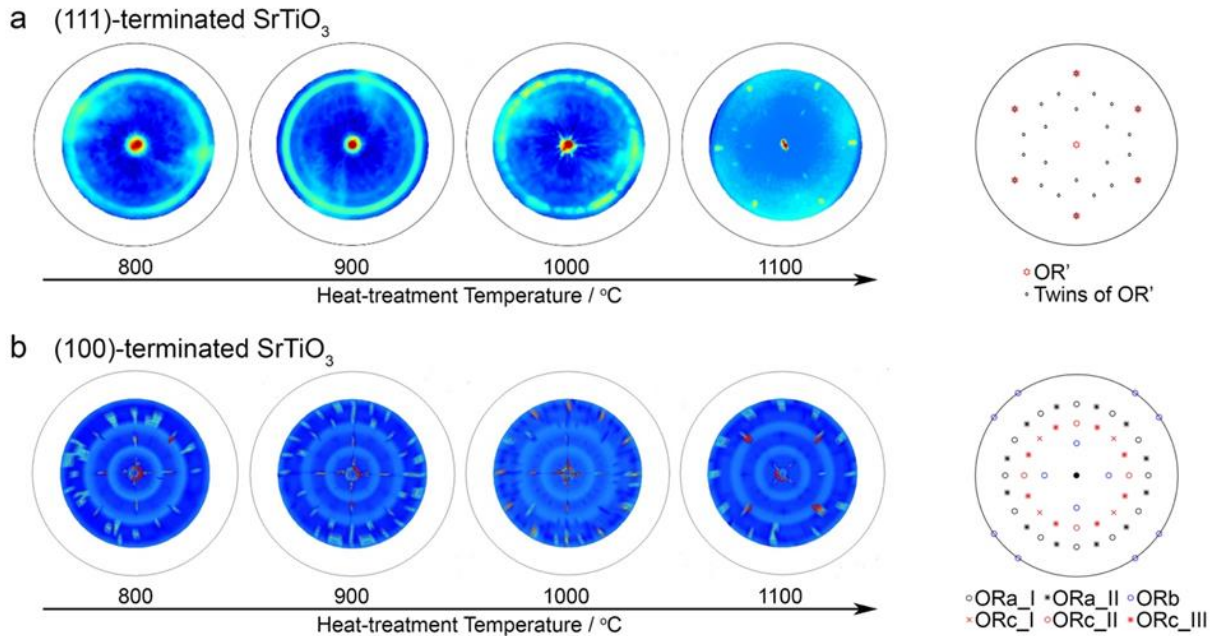


**Figure 3.**  $\{111\}$  Au pole figures measured by X-ray diffraction (XRD) for (111)-terminated  $\text{SrTiO}_3$  (a) and (100)-terminated  $\text{SrTiO}_3$  (b) substrates subjected to a heat treatment at 800, 900, 1000, and 1100 °C. The simulated pole figures based on the proposed ORs are shown to further support these ORs.

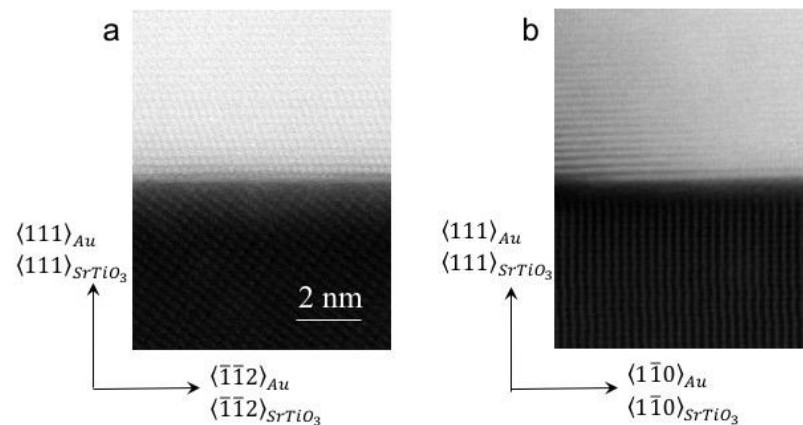
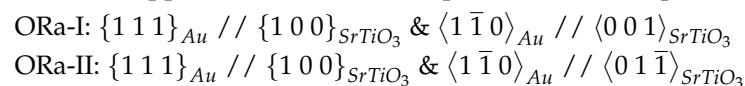


**Figure 4.** Atomically flat interface between Au particles and  $\text{SrTiO}_3$  substrates. The STEM-HAADF (scanning transmission electron microscopy-high-angle annular dark-field) images were viewed from  $\langle 1 \bar{1} 0 \rangle_{\text{Au}} // \langle 1 \bar{1} 0 \rangle_{\text{SrTiO}_3}$  (a) and  $\langle \bar{1} \bar{1} 2 \rangle_{\text{Au}} // \langle \bar{1} \bar{1} 2 \rangle_{\text{SrTiO}_3}$  (b), respectively. Since HAADF images are Z-contrast images, Au appears much brighter compared to the  $\text{SrTiO}_3$  substrate because of its high atomic number Z.

On the other hand, the (100)-terminated  $\text{SrTiO}_3$  substrate clearly holds (111)-, (110)-, and (100)-oriented Au particles from 800 °C to 1000 °C, while (110)-oriented Au particles almost disappear at 1100 °C. All Au particles maintain preferential ORs, including



$$\begin{aligned} \text{ORb: } & \{110\}_{\text{Au}} // \{100\}_{\text{SrTiO}_3} \ \& \ \langle 001 \rangle_{\text{Au}} // \langle 001 \rangle_{\text{SrTiO}_3} \\ \text{ORc-I: } & \{100\}_{\text{Au}} // \{100\}_{\text{SrTiO}_3} \ \& \ \langle 001 \rangle_{\text{Au}} // \langle 001 \rangle_{\text{SrTiO}_3} \\ \text{ORc-II: } & \{100\}_{\text{Au}} // \{100\}_{\text{SrTiO}_3} \ \& \ \langle 011 \rangle_{\text{Au}} // \langle 001 \rangle_{\text{SrTiO}_3} \\ \text{ORc-III: } & \{100\}_{\text{Au}} // \{100\}_{\text{SrTiO}_3} \ \& \ \langle 013 \rangle_{\text{Au}} // \langle 001 \rangle_{\text{SrTiO}_3} \end{aligned}$$

ORa-I contributes from 900 °C to 1100 °C; ORa-II only appears at 900 °C; ORb is favorable except at 1100 °C; all ORcs are found at 800 °C and 900 °C with only ORc-I dominating at 1100 °C. The above preferential ORs and their in-plane alignments usually suggest lower interfacial energies compared to the cases of identically oriented particles with random in-plane alignments, as evidenced by the evolution of random in-plane orientations to OR' in Figure 3a. The coexistence of (111)- and (100)-oriented Au particles, with ORa-I [28], ORa-II [9,25,28], and ORc-I [9,25], has been reported, although the other ORs are rarely mentioned in previous studies. In addition, no atomic reconstruction is observed at these interfaces with different ORs at high heat treatment temperatures [9,25], excluding the possibility of significant changes in interfacial energies for identical ORs under different heat treatment temperatures. Thus, under the condition of similar energy differences (i.e., very similar  $R_1/R_2$  ratio), the absence of (110)-oriented Au particles at 1100 °C may be due to the fact that the total energy of the  $\{110\}_{\text{Au}}$  orientation is slightly larger than those of other orientations (as shown in Figure 2d) and a high possibility of tuning orientations of Au particles at such high temperature. Our results demonstrate the possibility of tuning orientations of nanoparticles by heat treatment conditions. This suggests a possible synthesis condition of target-oriented nanoparticles.

The aforementioned discussion verified the necessity of using the law of energy minimization but not the least interfacial energy to determine the interface orientations. However, it should be noted that only a qualitative comparison based on the Winterbottom construction was conducted in the current work; a further coupling of this method to the density functional calculation and ab initio thermodynamics [29] can consider the influence of reaction conditions, but it is beyond the scope of this study.

#### 4. Conclusions

In the present work, theoretical and experimental efforts have been devoted to elucidating the orientation selection of FCC particles on crystalline substrates. Using dewetted Au particles on SrTiO<sub>3</sub> substrates with different terminations as the model system, we quantitatively demonstrated that preferential orientations correspond to interfaces with the best-matching of the closest-packed atomic planes, as in the case of (111)-oriented SrTiO<sub>3</sub>, and include multiple choices for similar contributions from both surface and interface energy, for example, multiple Au orientations on (100)-oriented SrTiO<sub>3</sub>. In summary, when the orientation of a supported nanoparticle is known as a prior, this particle can be well defined by inputting the interfacial energy into the Wulff–Kaisew construction; on the other hand, the preferential orientations of nanoparticles can be tuned by varying the interfacial energy, e.g., through the selection of substrate terminations. This work provides more robust guidance in the fabricating of special nanoparticles/substrate interfaces and targeting their orientation-dependent performance.

**Supplementary Materials:** The following are available online at <https://www.mdpi.com/article/10.3390/cryst12101414/s1>: Calculation equations for the change in energy. Figures S1 and S2: Evolution of the change of energy with the  $R_1/R_2$  from negative to positive  $R_1$  for 2D and 3D cases. Figure S3: Morphology of supported Au nanoparticles.

**Author Contributions:** This work has been carried out by W.K. and G.Z.; All authors have read and agreed to the published version of the manuscript.

**Funding:** This work was funded by the Canada Research Chair Program and the University of Manitoba.

**Acknowledgments:** The authors thank Anchao Yi for preparing test samples. W.K. is grateful to the China Scholarship Council (CSC201806290069) for the financial support during his study in Canada.

**Conflicts of Interest:** The authors declare no conflict of interest.

## References

1. Enterkin, J.A.; Setthapun, W.; Elam, J.W.; Christensen, S.T.; Rabuffetti, F.A.; Marks, L.D.; Stair, P.C.; Poepfelmeier, K.R.; Marshall, C.L. Propane oxidation over Pt/SrTiO<sub>3</sub> nanocuboids. *ACS Catal.* **2011**, *1*, 629–635. [[CrossRef](#)]
2. Green, I.X.; Tang, W.; Neurock, M.; Yates, J.T. Spectroscopic observation of dual catalytic sites during oxidation of CO on a Au/TiO<sub>2</sub> catalyst. *Science* **2011**, *333*, 736–739. [[CrossRef](#)] [[PubMed](#)]
3. Waser, R.; Dittmann, R.; Staikov, G.; Szot, K. Redox-based resistive switching memories—Nanoionic mechanisms, prospects, and challenges. *Adv. Mater.* **2009**, *21*, 2632–2663. [[CrossRef](#)]
4. Qin, W.; Hou, J.C.; Bonnell, D.A. Effect of interface atomic structure on the electronic properties of nano-sized metal–oxide interfaces. *Nano Lett.* **2015**, *15*, 211–217. [[CrossRef](#)] [[PubMed](#)]
5. Hagglund, C.; Zach, M.; Petersson, G.; Kasemo, B. Electromagnetic coupling of light into a silicon solar cell by nanodisk plasmons. *Appl. Phys. Lett.* **2008**, *92*, 053110. [[CrossRef](#)]
6. Brown, M.D.; Suteewong, T.; Kumar, R.S.S.; D’Innocenzo, V.; Petrozza, A.; Lee, M.M.; Wiesner, U.; Snaith, H.J. Plasmonic dye-sensitized solar cells using core-shell metalinsulator nanoparticle. *Nano Lett.* **2011**, *11*, 438–445. [[CrossRef](#)]
7. Cao, M.; Tang, Z.; Liu, Q.; Xu, Y.; Chen, M.; Lin, H.; Li, Y.; Gross, E.; Zhang, Q. The synergy between metal facet and oxide support facet for enhanced catalytic performance: The case of Pd–TiO<sub>2</sub>. *Nano Lett.* **2016**, *16*, 5298–5302. [[CrossRef](#)]
8. Li, X.R.; Ge, Z.C.; Xue, F.; Liu, H.; Lyu, B.; Liu, M.C. Lattice-oriented contact in Pd/SrTiO<sub>3</sub> heterojunction for rapid electron transfer during photocatalytic H<sub>2</sub> production. *Mater. Res. Bull.* **2020**, *123*, 110722. [[CrossRef](#)]
9. Kraya, R.; Kraya, L.Y.; Bonnell, D.A. Orientation controlled schottky barrier formation at Au nanoparticle–SrTiO<sub>3</sub> interfaces. *Nano Lett.* **2010**, *10*, 1224–1228. [[CrossRef](#)] [[PubMed](#)]
10. Shi, X.; Li, X.W.; Toda, T.; Oshikiri, T.; Ueno, K.; Suzuki, K.; Murakoshi, K.; Misawa, H. Interfacial structure-modulated plasmon-induced water oxidation on strontium titanate. *Appl. Energy Mater.* **2020**, *3*, 5675–5683. [[CrossRef](#)]
11. Barmparis, G.D.; Lodziana, Z.; Lopez, N.; Remediakis, L.N. Nanoparticle shapes by using Wulff constructions and first-principles calculations. *Beilstein J. Nanotechnol.* **2015**, *6*, 361–368. [[CrossRef](#)] [[PubMed](#)]
12. Honkala, K.; Hellman, A.; Remediakis, I.N.; Logadottir, A.; Carlsson, A.; Dahl, S.; Christensen, C.H.; Nørskov, J.K. Ammonia synthesis from first-principles calculations. *Science* **2005**, *307*, 555–558. [[CrossRef](#)] [[PubMed](#)]
13. Hellman, A.; Honkala, K.; Remediakis, I.N.; Logadóttir, Á.; Carlsson, A.; Dahl, S.; Christensen, C.H.; Nørskov, J.K. Insights into ammonia synthesis from first-principles. *Surf. Sci.* **2006**, *600*, 4264–4268. [[CrossRef](#)]
14. Kaishew, R. Sur la thermodynamique des germes cristallins. *Bull. Acad. Sci. Bulg. Ser. Phys.* **1951**, *2*, 191.
15. Winterbottom, W.L. Equilibrium shape of a small particle in contact with a foreign substrate. *Acta Metall.* **1967**, *15*, 303–310. [[CrossRef](#)]
16. Müller, P.; Kern, R. Equilibrium nano-shape changes induced by epitaxial stress (generalised Wulff–Kaishew theorem). *Surf. Sci.* **2000**, *457*, 229–253. [[CrossRef](#)]
17. Zhu, G.Z.; Majdi, T.; Shao, Y.; Bugnet, M.; Preston, J.S.; Botton, G. Atomic structure and bonding of the interfacial bilayer between Au nanoparticles and epitaxially regrown MgAl<sub>2</sub>O<sub>4</sub> substrates. *Appl. Phys. Lett.* **2014**, *105*, 231607. [[CrossRef](#)]
18. Majdi, T.; Zhu, G.Z.; Carvalho, J.; Jarvis, V.; Meinander, K.; Britten, J.F.; Botton, G.; Preston, J.S. Evidence for an equilibrium epitaxial complexion at the Au–MgAl<sub>2</sub>O<sub>4</sub> interface. *Appl. Phys. Lett.* **2015**, *107*, 241601. [[CrossRef](#)]
19. Lin, M.; Zhou, W.; Gu, X.; Zhu, G. Gold-rutile interfaces with irrational crystallographic orientations. *Mater. Charact.* **2021**, *176*, 11116. [[CrossRef](#)]
20. Chatterjee, D.; Kamalnath, A.R.K.; Ahmad, R.; Singh, A.K.; Ravishankar, N. Orientation selection during heterogeneous nucleation: Implications for heterogeneous catalysis. *J. Phys. Chem. C* **2017**, *121*, 10027–10037. [[CrossRef](#)]
21. Chen, P.; Murugappan, K.; Castell, M.R. Shapes of epitaxial gold nanocrystals on SrTiO<sub>3</sub> Substrates. *Phys. Chem. Chem. Phys.* **2020**, *22*, 4416–4428. [[CrossRef](#)] [[PubMed](#)]
22. Yi, A.C.; Liu, F.; Xie, D.Y.; Wen, M.; Zhu, G.Z. Gold-assisted growth of oxide bases underneath dewetted gold nanoparticles. *Mater. Charact.* **2019**, *151*, 237–241. [[CrossRef](#)]
23. Yao, S.Y.; Wen, M.; Zhu, G.Z. Bimodal size distribution of dewetted gold nanoparticles with regrown oxide bases. *Appl. Surf. Sci.* **2020**, *501*, 144227. [[CrossRef](#)]
24. Vitos, L.; Ruban, A.V.; Skriver, H.L.; Kollar, J. The surface energy of metals. *Surf. Sci.* **1998**, *411*, 186–202. [[CrossRef](#)]
25. Hou, J.; Nonnenmann, S.S.; Qin, W.; Bonnell, D.A. Size dependence of resistive switching at nanoscale metal-oxide interfaces. *Adv. Funct. Mater.* **2014**, *24*, 4113–4118. [[CrossRef](#)]
26. Liu, F.; Xie, D.Y.; Bugnet, M.; Majdi, T.; Preston, J.S.; Wang, J.; Zhu, G.Z. Temperature induced atomic reconstruction at Au/MgAl<sub>2</sub>O<sub>4</sub> interfaces. *Adv. Mater. Interfaces* **2018**, *5*, 1701664. [[CrossRef](#)]
27. Liu, F.; Xie, D.Y.; Majdi, T.; Zhu, G.Z. Twin-assisted growth of nominally stable substrates underneath dewetted Au nanoparticles. *Mater. Charact.* **2016**, *113*, 67–70. [[CrossRef](#)]
28. Silly, F.; Castell, M.R. Bimodal growth of Au on SrTiO<sub>3</sub> (001). *Phys. Rev. Lett.* **2006**, *96*, 086104. [[CrossRef](#)] [[PubMed](#)]
29. Cheula, R.; Soon, A.; Maestri, M. Prediction of morphological changes of catalyst materials under reaction conditions by combined ab initio thermodynamics and microkinetic modelling. *Catal. Sci. Technol.* **2018**, *8*, 3493–3503. [[CrossRef](#)] [[PubMed](#)]